Simultaneous Multislice Triple-Echo Steady-State (SMS-TESS) T$_1$, T$_2$, PD, and Off-Resonance Mapping in the Human Brain

Rahel Heule[1,2], Zarko Celicanin[1,2], Sebastian Kozerke[3], and Oliver Bieri[1,2]

[1]*Division of Radiological Physics, Department of Radiology, University Hospital Basel, University of Basel, Basel, Switzerland.*

[2]*Department of Biomedical Engineering, University of Basel, Basel, Switzerland.*

[3]*Institute for Biomedical Engineering, University and ETH Zurich, Zurich, Switzerland.*

Word count: 196 (Abstract), 5000 (Body), 9 Figures, 1 Table, 34 References, Supporting Information including text, 1 Supporting Information Table, and 3 Supporting Information Figures.

Correspondence to:

Rahel Heule, PhD

Division of Radiological Physics

Department of Radiology

University Hospital Basel, University of Basel

Petersgraben 4

4031 Basel, Switzerland

Email: rahel.heule@tuebingen.mpg.de

Phone: +41-61-556-5727

Fax: +41-61-265-4348

Running title: SMS-TESS T$_1$, T$_2$, PD, and Off-Resonance Mapping.

ABSTRACT

Purpose: To investigate the ability of simultaneous multislice triple-echo steady-state (SMS-TESS) imaging to provide quantitative maps of multiple tissue parameters, i.e., longitudinal and transverse relaxation times (T_1 and T_2), proton density (PD), and off-resonance (ΔB_0), in the human brain at 3 T from a single scan.

Methods: TESS acquisitions were performed in 2D mode to reduce motion sensitivity and accelerated by a simultaneous multislice excitation scheme (CAIPIRINHA) with SENSE reconstruction. SMS-acceleration factors (R) of 2 and 4 were evaluated. The *in vitro* and *in vivo* validation process included standard reference scans to analyze the accuracy of T_1, T_2, and ΔB_0 estimates, as well as single-slice TESS measurements.

Results: For R=2, the quantification of T_1, T_2, PD, and ΔB_0 was overall reliable with marginal noise enhancement. T_1 and T_2 values were in good agreement with the reference measurements and single-slice TESS. For R=4, the agreement of ΔB_0 with the standard reference was excellent and the determination of T_1, T_2, and PD was reproducible, however, increased variations in T_1 and T_2 values with respect to single-slice TESS were observed.

Conclusion: SMS-TESS has shown potential to offer rapid simultaneous T_1, T_2, PD, and ΔB_0 mapping of human brain tissues.

Keywords (3-6): triple-echo steady state (TESS); simultaneous multislice (SMS); multiparametric mapping; human brain tissues.

INTRODUCTION

The development of quantitative MR techniques for tissue characterization which are not only accurate and reproducible but also fast enough to meet clinical requirements regarding acquisition speed is challenging. Quantitative methods generally show a high sensitivity to MR hardware imperfections and are often limited to the estimation of a single tissue parameter. Fast MR acquisitions such as multiecho spin echo (ME-SE) (1-3) or steady-state free precession (SSFP) (4) typically produce an MR signal that depends on various tissue parameters and on the protocol setup. Therefore, multiparametric mapping is beneficial to accurately characterize several material parameters simultaneously without confounding bias. However, mapping of multiple tissue parameters based on conventional MR imaging commonly leads to prohibitively long scan times hindering clinical applications. It is thus not surprising that to date qualitative morphological MRI has remained the standard in clinical settings.

Magnetic resonance fingerprinting (MRF) has recently been presented as a novel MR acquisition and postprocessing concept for simultaneous multiparametric tissue determination (5). Following the introduction of MRF, many research studies have focused on exploring MRF acquisitions with pseudo-randomized acquisition parameters such as repetition time (TR) and/or flip angle (α) in different anatomical regions for simultaneous mapping of material-specific parameters, e.g., longitudinal (T_1) and transverse (T_2) relaxation times, proton density (PD), and/or off-resonance frequency (ΔB_0) (6-8).

Another new MR imaging approach which was suggested for the rapid simultaneous characterization of multiple tissue parameters is termed triple-echo steady-state (TESS). Initially, TESS has been proposed for the simultaneous quantification of the T_1 and T_2 relaxation times in the musculoskeletal system (9). After the original study, TESS was mainly investigated as a particularly robust and intrinsically B_1^+-insensitive method for T_2 relaxation time mapping in the knee (10), hip (11), wrist (12), and brain (13,14). While these studies focused on the estimation of a single tissue property (T_2), in principle, the magnitude and phase of the three SSFP contrasts, acquired with a single TESS measurement, offer information about four material properties, i.e., T_1, T_2, PD, and off-resonance frequency.

In the present work, the potential of TESS for fast simultaneous multiparametric (T_1, T_2, PD, and ΔB_0) mapping of human brain tissues from a single scan is explored. The TESS acquisitions are performed in 2D mode to mitigate motion sensitivity arising from cerebrospinal fluid (CSF) pulsations in the brain. The data acquisition is accelerated by simultaneous multislice (SMS) imaging using CAIPIRINHA to excite multiple slices simultaneously. Acceleration factors of 2 and 4 are investigated *in vitro* as well as *in vivo* at a field strength of 3 T.

METHODS

The postprocessing and visualization of the acquired MR data was implemented in MATLAB R2015b (The MathWorks, Inc., Natick, MA). The MR measurements were performed on a 3 T clinical scanner (Magnetom Prisma, Siemens Healthcare, Erlangen, Germany) and approved by the local ethics committee. The data presented in this work were acquired in six healthy subjects.

SMS-TESS Imaging

A dedicated 2D TESS sequence was adapted for SMS imaging as depicted in Figure 1. The three SSFP contrasts (F_1, F_0, F_{-1}) were acquired individually within separate radiofrequency (RF) cycles (i.e., each contrast within one TR, cf. Fig. 1a) to keep TR short as recently proposed for TESS imaging in the human brain at high field strength (13). Alternating multiband RF pulses similar to Hadamard pulses were implemented following the concept of CAIPIRINHA (15) to label each slice with a well-defined phase-cycle along the phase-encoding direction. Thereby, superimposed slices were produced with controlled field-of-view (FOV) shift. SMS-acceleration factors (corresponding to the number of simultaneously excited slices) of R=2 and R=4 were employed. The respective RF phase modulations which were used to achieve acceleration factors of 2 and 4 are noted in Figure 1b. As the three TESS base images were not acquired in the same but individual TRs, in the case of R=4, an RF phase increment of $3\pi/2$ (not $\pi/2$ as in conventional CAIPIRINHA) was needed to shift the respective slice by FOV/4, and an increment of $\pi/2$ (not $3\pi/2$ as in conventional CAIPIRINHA) to shift the respective slice by 3FOV/4 (cf. Fig. 1b). The multiband RF pulses were generated as the sum of single-band Hanning-windowed apodized SINC pulses with a duration of 4000 μs and a time-bandwidth-product of 2.

SMS-TESS imaging was performed at 3 T *in vitro* in five manganese-doped aqueous probes ([0.5, 0.25, 0.125, 0.05, 0.025] mM $MnCl_2$ in H_2O) covering a complete range of relevant T_1 and T_2 values, and *in vivo* in the human brain using the following parameters: TR = 9.84 ms, TE = TR/2 = 4.92 ms (in-phase), α_{nom} = 25° (nominal flip angle), receive bandwidth: 370 Hz/pixel, slice thickness: 4 mm. For the *in vitro* / *in vivo* scans, the in-plane resolution was set to 2 x 2 mm^2 (matrix size: 128 x 112) / 1.2 x 1.2 mm^2 (matrix size: 208 x 156). Six averages were taken to provide sufficient SNR in the TESS base images and to further mitigate motion issues related to the CSF pulsations in the brain, resulting in a total scan time of 20 s (*in vitro*) / 28 s (*in vivo*) for both 2- and 4-slice CAIPIRINHA acquisitions. Consequently, the acquisition time per slice was 10 s (*in vitro*) / 14 s (*in vivo*) and 5 s (*in vitro*) / 7 s (*in vivo*) for R=2 and R=4, respectively.

For SMS-TESS imaging with R=2, a center-to-center slice distance of 8 mm was used in combination with the standard 20-channel receive birdcage head coil of the manufacturer. To reduce the g-factor, SMS-TESS scans with R=4 were performed using an increased center-to-center slice distance of 20 mm and a standard 64-channel birdcage head coil. Since the neck coil elements were not selected, the net coil array size was 16 and 52 for R=2 and R=4, respectively.

SENSE Reconstruction

The aliased TESS images were unfolded using SENSE (16). The coil sensitivity maps required for the SENSE reconstruction were estimated with a "sum-of-squares" normalization from 2D spoiled gradient echo (SPGR) scans matching the slices acquired with SMS-TESS (relevant SPGR sequence parameters: TR = 4.9 ms, TE = 2.46 ms (in-phase), α = 8°, scan duration: ≈ 4.5 s / slice). Noise decorrelation was applied to both the raw TESS and SPGR data. The SENSE reconstruction was performed with Tikhonov regularization (17) for the SMS-TESS data obtained with an acceleration factor of R=4 to reduce the increased noise enhancement induced by the g-factor.

Using SMS imaging with R=2 and R=4, spatial coverage could be increased by factors of 2 and 4 relative to single-slice 2D TESS imaging. The scan time was kept equal for both employed acceleration factors (2 and 4) and in case of the *in vivo* scans similar to the single-slice 2D TESS protocol described in Ref. (13). The relative SNR in comparison to the unaccelerated case was calculated according to $SNR_{CAIPIRINHA}/SNR_{unaccelerated}$ =

$1/g(x)_{\text{CAIPIRINHA}}$ ($g(x)_{\text{CAIPIRINHA}}$: spatially dependent g-factor of the SENSE reconstruction) (15).

Multiparametric TESS Mapping

For human brain tissue characterization, the unaliased TESS base images (F_1, F_0, F_{-1}) were skull-stripped using the brain extraction tool (BET) provided by the software package FSL (18). The T_1 and T_2 relaxation times were determined according to the principle of 2D TESS relaxometry (13). The (non-rectangular) slice profile was calculated as the inverse Fourier transform of the RF pulse envelope (Fourier transform approximation). This approximation holds well for small flip angles as employed in this work and gives an estimate of the flip angle distribution across the slice (19). Accordingly, the accumulated signal of the SSFP modes acquired with 2D TESS is given by the sum

$$\hat{F}_{1,0,-1} := \sum_{i=1}^{N} F_{1,0,-1}(\alpha_i) \qquad [1]$$

where α_i represents the discrete sample points of the flip angle distribution (slice profile) (13). Estimates for T_1 and T_2 were then obtained in an iterative approach, by using the sensitivity of the signal ratio $\hat{F}_1/\hat{F}_0$ to T_1 and the sensitivity of the signal ratio $\hat{F}_{-1}/(\hat{F}_0 - \hat{F}_1)$ to T_2. More details on TESS-based relaxometry are available in Refs. (13) (2D TESS) and (9) (3D TESS).

While TESS-T_2 was reported to be intrinsically insensitive to transmit field (B_1^+) inhomogeneity (9,13), B_1^+-correction is crucial for accurate T_1 quantification with TESS. The standard B_1^+ mapping sequence available as product implementation on Siemens platforms was used for the calculation of B_1^+ maps. It employs a preconditioning RF pulse in combination with a TurboFLASH readout (20,21). TESS imaging was thus accompanied by a fast B_1^+ mapping scan (number of acquired slices: 11, slice thickness: 4 mm, in-plane resolution: 4 x 4 mm^2, scan duration: 8 s). The B_1^+-corrected flip angle sample points were then derived as $\alpha_i = c_{B_1} \cdot \alpha_{i,nom}$, where c_{B_1} is the B_1^+ scaling factor obtained from the B_1^+ mapping scan and $\alpha_{i,nom}$ refers to the flip angle distribution calculated for the nominal flip angle ($\alpha_{nom} = 25°$). To eliminate the B_1^+-bias in the TESS-T_1 quantification, Eq. [1] was modified to take into account the B_1^+-corrected flip angle sample points:

$$\hat{F}_{1,0,-1} := \sum_{i=1}^{N} F_{1,0,-1}(c_{B_1} \cdot \alpha_{i,nom}) \qquad [2]$$

PD maps were calculated based on the F_0 signal amplitude with B_1^+-corrected T_1 and T_2 values estimated by TESS relaxometry: $\hat{F}_0 = \hat{F}_0(T_{1,TESS}, T_{2,TESS}, c_{B_1} \cdot \alpha_{i,nom})$. The receiver coil sensitivity profile was corrected from the coil sensitivity calibration scan.

Off-resonance frequency distribution (ΔB_0) was estimated by making use of the different phase evolutions of the transverse steady-state configurations F_{-1}, F_0, and F_1. The F_{-1} state can be considered as a time-reversed F_0 state with an effective echo time of $-TE$. The F_1 state results from the excitation by the RF pulse in the previous sequence cycle with an effective echo time of $TR+TE$. As a result, in the presence of an off-resonance frequency $\Delta\omega$, the series [F_{-1}, F_0, F_1] is subject to an equidistant phase increment of $\Delta\omega \cdot TR$. The off-resonance frequency $\Delta\omega$ can then be extracted by performing a matrix pencil analysis (22) assuming a single pole on the complex SSFP signal series [F_{-1}, F_0, F_1]. Wraps in the calculated off-resonance maps were removed using a 2D phase unwrapping algorithm (23) assuming the true reference phase in the center of the phantom / brain. In a last step, the off-resonance maps were spatially smoothed with a 2D median filter (window size: 9).

Assessment of Accuracy and Reproducibility

SMS-TESS T_1 and T_2 values were validated against standard reference data *in vitro* for both R=2 and R=4 in a manganese-doped probe (0.125 mM $MnCl_2$ in H_2O) as well as *in vivo* for R=2 in volunteer 1. The reference T_1 was measured based on six single-slice inversion-recovery turbo-spin-echo (IR-TSE) scans with a TR of 10 s and inversion times of TI = [100, 200, 400, 800, 1600, 3200] ms by nonlinear least-squares fitting of the acquired data sets. The reference T_2 was obtained from six single-slice single-echo spin-echo (SE) scans with a TR of 6000 ms (*in vitro*) / 1500 ms (*in vivo*) and echo times of TE = [10, 20, 40, 60, 100, 150] ms using nonlinear least-squares fitting. For the *in vivo* validation, it was ensured to match the image position of the reference slice with slice 2 imaged by SMS-TESS (R=2). The T_1 and T_2 accuracy of SMS-TESS was assessed *in vitro* for circular regions-of-interest (ROIs) (cf. Fig. 2) and *in vivo* for selected ROIs in white and gray matter structures in the human brain (cf. Fig. 5b). In the same anatomical regions as indicated in Fig. 5b for R=2, ROIs were drawn on slice 4 of the R=4 data set of volunteer 1 to assess T_1 and T_2 values (note that the positioning of slice 4, R=4 and slice 2, R=2 is not exactly the same).

The SMS-TESS ΔB_0 validation against standard dual-echo field mapping is presented for R=4 both *in vitro* (0.125 mM $MnCl_2$ in H_2O) as well as *in vivo* in volunteer 2. The dual-echo gradient echo reference scan was performed with TR = 400 ms, TE_1 = 4.92 ms, TE_2 = 7.38 ms, and α_{nom} = 60°. *In vitro*, an offset was added to the shim gradient in x-direction after B_0 field adjustment to increase the off-resonance variation in the phantom (linear increase across the FOV from left to right). *In vivo*, the agreement with the reference measurement was visually analyzed for a selected slice by a correlation scatter plot using linear least-squares fitting and quantified by the gold standard correlation coefficient (r_{GCC}) (24). No special shimming was performed *in vivo* for the validation of the proposed off-resonance mapping method to assess larger B_0 variations.

The agreement of SMS-TESS T_1 and T_2 quantification with standard reference data was further assessed in a phantom with four different T_1 / T_2 compartments in the range of physiological values, containing varying concentrations of $MnCl_2$ diluted in water (more details are given in the Supporting Information).

In vivo reproducibility of SMS-TESS T_1, T_2, and PD was examined for R=4 by 10 consecutive measurements of volunteer 2. After each measurement, the volunteer was taken out from the scanner and repositioned to enforce new scan conditions for the subsequent acquisitions. The Siemens AutoAlign feature was used to ensure automatic alignment of the slice positions in a reproducible way. Quantitatively, the T_1, T_2, and PD reproducibility was assessed on slice 4 for a ROI in white matter (frontal) as well as a ROI in gray matter (putamen) (cf. Supporting Information Figure S1 for the definition of the ROIs) and quantified by the coefficient of variation (cv) defined as the standard deviation divided by the mean.

The consistency of the derived SMS-TESS T_1 and T_2 values was validated *in vitro* in five manganese-doped aqueous probes ([0.5, 0.25, 0.125, 0.05, 0.025] mM $MnCl_2$ in H_2O) as well as *in vivo* in four healthy subjects (volunteers 3, 4, 5, and 6) for R=2 and R=4 against single-slice TESS scans. The imaging parameters of SMS-TESS and single-slice TESS were completely identical; consequently the scan time per slice was 20 s (*in vitro*) / 28 s (*in vivo*) for the single-slice TESS acquisitions. *In vitro*, circular ROIs covering a large extent of the probes were drawn on all acquired slices and the agreement between the two methods was analyzed by the calculation of the intraclass correlation coefficient (ICC) (25) as well as

linear least-squares fitting. *In vivo*, ROIs were selected on all slices in anatomical structures that were consistently visible in all four subjects. The location of the ROIs is illustrated on the unfolded F_{-1} base images acquired in volunteer 6 (cf. Supporting Information Figure S2).

RESULTS

In vitro, nominal reference T_1 and T_2 values of 879 ± 2 ms and 70.1 ± 0.1 ms, respectively, are obtained for the assessed probe (0.125 mM $MnCl_2$ in H_2O). SMS-TESS relaxometry with R=2 yields mean values of T_1 = 895 ± 39 ms and T_2 = 70.1 ± 1.6 ms averaged over both slices. For R=4, averaging over all four slices yields mean values of T_1 = 879 ± 43 ms and T_2 = 70.2 ± 2.1 ms. The T_1 and T_2 values of the individual four slices are displayed in Figure 2 (rows 2 and 3) revealing that T_1 is slightly increasing from slice 1 (861 ± 18 ms) to slice 4 (887 ± 41 ms). Overall, the deviation of assessed mean T_1 and T_2 values of the individual slices acquired with acceleration factors of 2 and 4 from the nominal reference values is ≤ 2% for T_1 and ≤ 1% for T_2. For R=2, assessed mean / peak g-factors are: 1.03 / 1.32 (slice 1) and 1.03 / 1.29 (slice 2); for R=4: 1.05 / 1.16 (slice 1), 1.09 / 1.27 (slice 2), 1.13 / 1.34 (slice 3), and 1.08 / 1.25 (slice 4). Excellent agreement is found between SMS-TESS ΔB_0 employing R=4 and the reference measurement (cf. Fig. 2, rows 4 and 5).

In a phantom consisting of four vials with different nominal T_1 and T_2 values, SMS-TESS with R=2 yields T_1 and T_2 estimates that deviate on average only about 3.5% and 2.1% from the reference T_1 and T_2, respectively (cf. Supporting Information Table S1). Increased deviations from the reference data are observed for SMS-TESS with R=4; on average about 7.5% and 5.5% for T_1 and T_2, respectively (cf. Supporting Information Table S1).

In Figure 3, the results of the *in vitro* T_1 and T_2 comparison between SMS-TESS and single-slice TESS are visualized. Excellent agreement is observed between the T_1 and T_2 values obtained with unaccelerated TESS and R=2 SMS-TESS for both acquired slices as reflected by high ICC values and slope values of the linear fit that are almost equal to 1 (cf. Fig. 3a). The comparison between unaccelerated TESS and R=4 SMS-TESS yields high ICC values, however, increasing deviation can be observed of the linear fit (solid black lines) from the ideal agreement (dotted red lines) with longer T_1 and T_2 values (cf. Fig. 3b), in particular for

slices 2 and 3 where the mean and peak g-factors are higher (mean / peak g-factors across all five probes: 1.04 / 1.14, 1.10 / 1.31, 1.15 / 1.35, 1.09 / 1.26 for slices 1, 2, 3, 4, respectively).

In vivo, SMS-TESS imaging with R=2 is demonstrated for human brain scans in volunteer 1 at 3 T (cf. Fig. 4). The unfolded base TESS contrasts (F_1, F_0, and F_{-1}) are of high quality without any visible reconstruction related degradation (cf. Fig. 4, rows 2 and 3). An average g-factor of 1.01 is obtained for both slices resulting in a mean relative SNR of 0.99 with respect to the unaccelerated case (see the corresponding g-factor maps in Fig. 4, last column). For both slices, the peak g-factor is 1.22.

The T_1, T_2, PD, and ΔB_0 maps calculated from the SENSE-reconstructed TESS base images (cf. Fig. 4) are provided in Figure 5a and prove the feasibility of multiparametric TESS imaging in the human brain with an SMS acceleration factor of 2. The validation of SMS-TESS T_1 relaxometry against inversion-recovery T_1 measurements for the ROIs indicated in Figure 5b yields the following TESS-T_1 values with the reference values given in brackets: 862 ± 50 ms (863 ± 21 ms) for WM_1, 871 ± 77 ms (901 ± 38 ms) for WM_2, 1335 ± 235 ms (1245 ± 84 ms) for GM_1, and 1378 ± 212 ms (1211 ± 39 ms) for GM_2. While in the white matter structures good agreement between TESS-T_1 and the reference method is found, a slight T_1 overestimation and increased standard deviations are observed in gray matter. For SMS-TESS T_2 quantification with R=2, an overall good agreement with standard single-echo spin-echo T_2 data is found as reflected by the assessed values (reference values given in brackets): 49 ± 3 ms (52 ± 3 ms) for WM_1, 51 ± 4 ms (59 ± 5 ms) for WM_2, 47 ± 4 ms (46 ± 2 ms) for GM_1, and 43 ± 3 ms (43 ± 3) for GM_2.

The potential of SMS-TESS imaging is exploited by investigating the simultaneous excitation of four slices in volunteer 1 (cf. Figs. 6 and 7). Despite the high acceleration, the results of the SENSE reconstruction shown in Figure 6 for a representative data set acquired at 3 T reveal unfolded TESS base images of good quality with only a moderate g-factor related noise enhancement (the corresponding aliased data are provided in the Supporting Information Figure S3). Mean g-factor values of 1.06, 1.09, 1.13, and 1.08 are found for slices 1, 2, 3, and 4, respectively (cf. Fig. 6, last column) yielding a mean g-factor of 1.09 averaged over all four slices with a respective mean relative SNR of 0.92. Peak g-factors are 1.19, 1.29, 1.37, and 1.29 as assessed for slices 1, 2, 3, and 4, respectively. The corresponding

quantitative T_1, T_2, PD, and ΔB_0 maps are displayed in Figure 7. The following T_1 / T_2 values are obtained in white and gray matter structures of volunteer 1 (Fig. 7, slice 4): 884 ± 35 ms / 50 ± 4 ms for WM_1, 874 ± 67 ms / 46 ± 2 ms for WM_2, 1475 ± 311 ms / 50 ± 6 ms for GM_1, and 1529 ± 310 ms / 45 ± 7 for GM_2.

Figure 8 illustrates the reproducibility assessment of SMS-TESS T_1, T_2, and PD mapping with R=4 in volunteer 2 on slice 4 (for the definition of the ROIs see the Supporting Information Figure S1). The mean g-factor calculated for this slice is 1.09 (peak value: 1.32). Note that the TESS F_1 contrast exhibits some susceptibility artifacts in regions close to the sinuses as pointed out by the white arrows in the Supporting Information Figure S1. In the white matter ROI, mean T_1 and T_2 values of 880 ± 20 ms and 49 ± 1 ms, respectively, are found over the course of 10 consecutive measurements resulting in a cv of 0.02 for both T_1 and T_2. In the gray matter ROI, a mean T_1 of 1443 ± 67 ms and a mean T_2 of 42 ± 1 ms, respectively, are obtained with cv = 0.05 (T_1) and cv = 0.03 (T_2). For PD, a mean white matter / gray matter ratio of 0.83 ± 0.01 with a cv = 0.02 is yielded in good agreement with literature values (26). *In vivo* comparison of SMS-TESS ΔB_0 versus the reference field mapping reveals an excellent agreement between both methods with a gold standard correlation coefficient of 0.995 calculated for volunteer 2 on slice 4 (cf. Fig. 9).

In Table 1, the results from a ROI T_1 and T_2 comparison between SMS-TESS (R=2 and R=4) and unaccelerated TESS in four healthy subjects (volunteers 3, 4, 5, 6) are summarized. For R=2, the mean T_1 and T_2 values of SMS-TESS assessed in the selected ROIs agree generally well with single-slice TESS and exhibit overall similar standard deviations. A slight but consistent underestimation of T_1 is observed in the WM ROI (ROI 1) while in the GM ROI (ROI 2) T_1 underestimation occurs for volunteers 3 and 4, and T_1 overestimation for volunteers 5 and 6 who exhibit generally increased T_1 values. The observed deviations are rather small; on average 5.1% / 1.8% (ROI 1) and 4.0% / 3.3% (ROI 2) for T_1 / T_2. For R=4, increased standard deviations of the mean T_1 and T_2 values are observed in regions affected by g-factor-induced noise enhancement as clearly apparent in ROI 2 and ROI 3 (cf. Table 1). In certain ROIs, noise enhancement is seen to lead to mean SMS-TESS T_1 and T_2 values that deviate considerably from the single-slice results, e.g., in volunteer 1 / R=4 / ROI 2, where deviations of 18.8% and 15.4% are observed for T_1 and T_2, respectively. Similarly to R=2,

SMS-TESS with R=4 tends to underestimate T_1 in white matter by about 5.7% on average across all volunteers and ROIs.

DISCUSSION

In this work, we suggest the use of a single triple-echo steady-state (TESS) scan to simultaneously quantify T_1, T_2, PD, and ΔB_0 of human brain tissues. Due to the nonbalanced characteristics of the TESS sequence, imaging was performed in 2D mode with a few averages to reduce the motion sensitivity arising from CSF pulsations in the brain. The high SNR provided in the TESS base images was used to accelerate the acquisitions by simultaneous excitation of multiple slices with CAIPIRINHA.

Multiband RF pulses with a low time-bandwidth-product of 2 were used to facilitate the multiband pulse implementation and the incorporation of the slice profile into TESS-based multiparametric mapping. Because the simultaneously excited slices were separated by a gap (center-to-center slice distance of 8 mm and 20 mm for R=2 and R=4, respectively), sideband excitation was not expected to impair the data reconstruction.

In vitro, good agreement was observed of SMS-TESS T_1 and T_2 mapping with the values obtained from standard reference scans for a manganese-doped probe with tissue-like relaxation times (0.125 mM $MnCl_2$ in H_2O). The slight increase of T_1 values apparent for R=4 across the four slices (cf. Fig. 2) is likely to be caused by some residual B_1^+ field related bias, corroborated by the behavior of T_2 values that are known to be B_1^+-insensitive and did not show any significant variation across the slices. As a result, also the small deviation (~ 2%) of the R=2 T_1 values from the reference measurement can possibly be attributed to a residual B_1^+ bias (resulting from a residual inaccuracy in the used B_1^+ mapping method). In a phantom with four different T_1 and T_2 compartments, SMS-TESS yielded overall good agreement with the reference T_1 and T_2 data, however, the noise enhancement due to the increased g-factor resulted in increased deviations in case of R=4 (cf., Supporting Information Table S1).

For an SMS acceleration factor of 2, the g-factor induced noise enhancement was marginal, thus preserving the SNR (relative SNR of the *in vivo* scans was 0.99 compared to the

unaccelerated case). To minimize the increase of the g-factor at higher acceleration (in this work R=4), an adapted measurement setup was investigated. A head coil with a larger number of channels was used (52 instead of 16 independent coil elements), the slice spacing in the SMS-TESS protocol was increased (from 8 to 20 mm center-to-center), and the SENSE reconstruction was employed with Tikhonov regularization. Thereby, the average g-factor for an acceleration factor of 4 could be reduced from initially about 1.7 (16 channels, 8 mm center-to-center slice spacing, no regularization) to 1.09 (assessed for volunteer 1). As a result, a high relative SNR of 0.92 in comparison to sequential single-slice imaging was obtained while at the same time the scan time was shortened by a factor of 4. The influence of the Tikhonov regularization was rather small and effected a decrease of the g-factor from 1.10 to 1.09 for volunteer 1.

The unaliased TESS contrasts acquired in volunteer 1 with R=2 and R=4 demonstrate good image quality (cf. Figs. 4 and 6). However, g-factor induced noise enhancement, even if subtle, can lead to a degradation of the quantitative maps. Furthermore, there are regions exhibiting locally increased g-values (e.g., in the case of volunteer 1 up to 1.22 at R=2 and 1.37 at R=4). The observed T_1 overestimation in gray matter structures in comparison to the reference method for R=2 is thus likely caused by g-factor related noise enhancement. Residual inaccuracy in the B_1^+ mapping method or the slice profile correction may also result in an overestimation of T_1.

The reproducibility analyzed for R=4 in volunteer 2 (cf. Fig. 8) was good in frontal white matter for both T_1 and T_2. However, note that the calculated coefficient of variation for T_2 was higher in comparison to single-slice TESS T_2 mapping (13) reflecting g-factor induced noise enhancement. Similarly, the PD white matter / gray matter ratio showed a low variability (cv = 0.02). Increased coefficients of variation were observed in the assessed gray matter ROI, especially for T_1. Apart from the g-factor, slight variations in the automatic alignment of the slice positions may contribute to the observed variability, in particular in the gray matter ROI where through-plane tissue variations might be larger.

Validation against single-slice TESS in four subjects revealed that SMS-TESS T_1 tends to be consistently underestimated in white matter while in gray matter also overestimation occurred (cf. Table 1). Overall, at both R=2 and R=4, the assessed SMS-TESS T_1 and T_2 values were in the range of reported literature values for all six measured volunteers (13,27-29). The

standard deviations of the mean T_1 and T_2 values in the assessed ROIs were comparable to single-slice TESS for R=2, thus indicating that the SNR of the T_1 and T_2 quantification was highly preserved. In case of R=4, the standard deviations of both T_1 and T_2 were clearly increased in certain ROIs (cf. Table 1) due to the higher g-factors.

For future work, it is crucial to achieve a further reduction of the g-factor. At R=4, the g-factor related noise enhancement was observed to vary considerably depending on the brain anatomy of the scanned subject and on the positioning of the head in the coil; leading to a subject-dependent impairment of T_1 and T_2 quantification as apparent from the comparison to single-slice TESS (cf. Table 1). Future investigations may thus focus on prior-driven reconstruction techniques taking into account anatomical and parametric prior information, e.g., anatomically-constrained inversion or dictionary-based fitting. To reduce the susceptibility sensitivity of the F_1 contrast (cf. Supporting Information Figure S1), shorter TR and advanced shimming techniques may be investigated. The motion sensitivity inherent to nonbalanced SSFP sequences may be further mitigated in future studies by combining TESS not only with acceleration in slice direction (here: CAIPIRINHA) but also in-plane in phase-encoding direction (using, e.g., GRAPPA (30)) while on the other hand increasing the number of averages.

The derived T_2 from SMS-TESS is insensitive to B_1, making it particularly interesting for ultra-high field applications. The B_1-bias inherent in the T_1 can be corrected by a B_1 mapping scan. In contrast, multiparametric techniques based on sampling the bSSFP profile (31,32) exhibit a considerable T_1 underestimation due to profile asymmetries, in particular in white matter, which cannot be resolved by B_1 mapping. Moreover, SMS-TESS does not require a series of measurements like other multiparametric methods (31-33) but allows to acquire three intrinsically co-registered contrasts from a single scan. While three contrasts are sufficient to quantify four parameters with SMS-TESS, MRF, on the other hand, analyzes several hundred signal time points. Thus, clinically acceptable scan times can only be reached if the acquisition is highly accelerated, i.e., by using spiral trajectories. In contrast, SMS-TESS can be acquired at high resolution based on a Cartesian trajectory. Regarding speed, SMS-TESS with acceleration factors of 2 and 4 showed potential to compete with other SMS-accelerated quantitative MR techniques like, e.g., t-Blipped SMS-MRF (34). In addition, similar to MRF, SMS-TESS could be further accelerated by incorporating non-Cartesian trajectories.

CONCLUSION

SMS-TESS imaging allows the rapid estimation of multiple tissue parameters (T_1, T_2, PD, and B_0) in the human brain by using the magnitude and phase information of three SSFP contrasts acquired in a single scan. The agreement with standard reference methods and literature was good for T_1, T_2, as well as PD and even excellent for B_0. While, at R=2, the SNR in the T_1 and T_2 quantification was highly preserved as reflected by similar standard deviations in the assessed ROIs in comparison to single-slice TESS, at R=4, the observed increased standard deviations indicate that a further reduction of the g-factor is crucial for reliable T_1 and T_2 mapping.

ACKNOWLEDGEMENT

REFERENCES

1.   Carr HY, Purcell EM. Effects of diffusion on free precession in nuclear magnetic resonance experiments. Phys Rev 1954;94(3):630-638.

2.   Meiboom S, Gill D. Modified spin-echo method for measuring nuclear relaxation times. Rev Sci Instrum 1958;29:688-691.

3.   Hennig J, Nauerth A, Friedburg H. RARE imaging: a fast imaging method for clinical MR. Magn Reson Med 1986;3(6):823-833.

4.   Carr HY. Steady-state free precession in nuclear magnetic resonance. Phys Rev 1958;112(5):1693-1701.

5.   Ma D, Gulani V, Seiberlich N, Liu K, Sunshine JL, Duerk JL, Griswold MA. Magnetic resonance fingerprinting. Nature 2013;495(7440):187-192.

6.   Chen Y, Jiang Y, Pahwa S, Ma D, Lu L, Twieg MD, Wright KL, Seiberlich N, Griswold MA, Gulani V. MR fingerprinting for rapid quantitative abdominal imaging. Radiology 2016;279(1):278-286.

7.   Hamilton JI, Jiang Y, Chen Y, Ma D, Lo WC, Griswold M, Seiberlich N. MR fingerprinting for rapid quantification of myocardial T1, T2, and proton spin density. Magn Reson Med 2017;77(4):1446-1458.

8.   Pierre EY, Ma D, Chen Y, Badve C, Griswold MA. Multiscale reconstruction for MR fingerprinting. Magn Reson Med 2016;75(6):2481-2492.

9.   Heule R, Ganter C, Bieri O. Triple echo steady-state (TESS) relaxometry. Magn Reson Med 2014;71(1):230-237.

10.   Juras V, Bohndorf K, Heule R, Kronnerwetter C, Szomolanyi P, Hager B, Bieri O, Zbyn S, Trattnig S. A comparison of multi-echo spin-echo and triple-echo steady-state T2 mapping for in vivo evaluation of articular cartilage. Eur Radiol 2016;26(6):1905-1912.

11.   Kraff O, Lazik-Palm A, Heule R, Theysohn JM, Bieri O, Quick HH. 7 Tesla quantitative hip MRI: a comparison between TESS and CPMG for T2 mapping. MAGMA 2016;29(3):503-512.

12.   Riegler G, Drlicek G, Kronnerwetter C, Heule R, Bieri O, Bodner G, Lieba-Samal D, Trattnig S. High-resolution axonal bundle (fascicle) assessment and triple-echo steady-state T2 mapping of the median nerve at 7 T: preliminary experience. Invest Radiol 2016;51(8):529-535.

13.   Heule R, Bar P, Mirkes C, Scheffler K, Trattnig S, Bieri O. Triple-echo steady-state T2 relaxometry of the human brain at high to ultra-high fields. NMR Biomed 2014;27(9):1037-1045.

14.   Pusterla O, Santini F, Heule R, Bieri O. T2-Snapshots imaging with simultaneous multislice TESS acquisition. Proceedings ISMRM 2015. p 441.

15.   Breuer FA, Blaimer M, Heidemann RM, Mueller MF, Griswold MA, Jakob PM. Controlled aliasing in parallel imaging results in higher acceleration (CAIPIRINHA) for multi-slice imaging. Magn Reson Med 2005;53(3):684-691.

16.   Pruessmann KP, Weiger M, Scheidegger MB, Boesiger P. SENSE: sensitivity encoding for fast MRI. Magn Reson Med 1999;42(5):952-962.

17.   Tikhonov AN. Regularization of incorrectly posed problems. Dokl Akad Nauk SSSR 1963;4(6):1624-1627.

18.   Smith SM, Jenkinson M, Woolrich MW, Beckmann CF, Behrens TEJ, Johansen-Berg H, Bannister PR, De Luca M, Drobnjak I, Flitney DE, Niazy RK, Saunders J, Vickers J, Zhang YY, De Stefano N, Brady JM, Matthews PM. Advances in functional and structural MR image analysis and implementation as FSL. Neuroimage 2004;23:S208-S219.

19.   Bernstein MA, King KF, Zhou XJ. Handbook of MRI Pulse Sequences. Burlington, MA: Elsevier Academic Press; 2004.

20.   Fautz HP, Vogel M, Gross P, Kerr A, Zhu Y. B1 mapping of coil arrays for parallel transmission. Proceedings ISMRM 2008. p 1247.

21.   Chung S, Kim D, Breton E, Axel L. Rapid B1+ mapping using a preconditioning RF pulse with TurboFLASH readout. Magn Reson Med 2010;64(2):439-446.

22.   Lin YY, Hodgkinson P, Ernst M, Pines A. A novel detection-estimation scheme for noisy NMR signals: Applications to delayed acquisition data. Journal of magnetic resonance 1997;128(1):30-41.

23.   Goldstein RM, Zebker HA, Werner CL. Satellite radar interferometry - two-dimensional phase unwrapping. Radio Sci 1988;23(4):713-720.

24.   Laurent RTS. Evaluating agreement with a gold standard in method comparison studies. Biometrics 1998;54:537-545.

25.   Shrout PE, Fleiss JL. Intraclass correlations: uses in assessing rater reliability. Psychol Bull 1979;86(2):420-428.

26.   Tofts PS. PD: Proton Density of Tissue Water. Quantitative MRI of the Brain: Measuring Changes Caused by Disease 2003:85-109.

27. Wansapura JP, Holland SK, Dunn RS, Ball WS, Jr. NMR relaxation times in the human brain at 3.0 Tesla. J Magn Reson Imaging 1999;9(4):531-538.

28. Stanisz GJ, Odrobina EE, Pun J, Escaravage M, Graham SJ, Bronskill MJ, Henkelman RM. T1, T2 relaxation and magnetization transfer in tissue at 3T. Magn Reson Med 2005;54(3):507-512.

29. Petrovic A, Scheurer E, Stollberger R. Closed-form solution for T2 mapping with nonideal refocusing of slice selective CPMG sequences. Magn Reson Med 2015;73(2):818-827.

30. Griswold MA, Jakob PM, Heidemann RM, Nittka M, Jellus V, Wang J, Kiefer B, Haase A. Generalized autocalibrating partially parallel acquisitions (GRAPPA). Magn Reson Med 2002;47(6):1202-1210.

31. Nguyen D, Bieri O. Motion-insensitive rapid configuration relaxometry. Magn Reson Med 2017;78(2):518-526.

32. Shcherbakova Y, van den Berg CAT, Moonen CTW, Bartels LW. PLANET: An ellipse fitting approach for simultaneous T1 and T2 mapping using phase-cycled balanced steady-state free precession. Magn Reson Med 2018;79(2):711-722.

33. Deoni SC, Rutt BK, Peters TM. Rapid combined T1 and T2 mapping using gradient recalled acquisition in the steady state. Magn Reson Med 2003;49(3):515-526.

34. Ye HH, Ma D, Jiang Y, Cauley SF, Du YP, Wald LL, Griswold MA, Setsompop K. Accelerating magnetic resonance fingerprinting (MRF) using t-blipped simultaneous multislice (SMS) acquisition. Magnet Reson Med 2016;75(5):2078-2085.

TABLE

		R=2		R=4			
		ROI 1	*ROI 2*	*ROI 1*	*ROI 2*	*ROI 3*	*ROI 4*
Volunteer 3	acc.	800 ± 73 / 44 ± 2	1215 ± 173 / 43 ± 4	853 ± 98 / 41 ± 4	789 ± 145 / 40 ± 5	731 ± 80 / 54 ± 5	951 ± 147 / 41 ± 3
	unacc.	862 ± 81 / 46 ± 2	1285 ± 155 / 46 ± 5	926 ± 95 / 42 ± 4	971 ± 63 / 47 ± 3	774 ± 52 / 49 ± 2	1057 ± 106 / 43 ± 2
Volunteer 4	acc.	736 ± 34 / 49 ± 2	1252 ± 156 / 48 ± 3	849 ± 111 / 48 ± 5	820 ± 162 / 48 ± 8	726 ± 79 / 56 ± 11	813 ± 124 / 45 ± 4
	unacc.	772 ± 39 / 51 ± 2	1291 ± 130 / 48 ± 3	864 ± 124 / 52 ± 5	829 ± 87 / 51 ± 3	737 ± 49 / 49 ± 2	918 ± 92 / 46 ± 3
Volunteer 5	acc.	815 ± 65 / 49 ± 3	1317 ± 130 / 49 ± 5	979 ± 72 / 50 ± 3	824 ± 79 / 54 ± 5	812 ± 73 / 56 ± 8	833 ± 54 / 47 ± 3
	unacc.	845 ± 69 / 50 ± 2	1299 ± 135 / 49 ± 4	999 ± 80 / 49 ± 4	856 ± 53 / 54 ± 3	848 ± 74 / 51 ± 3	879 ± 80 / 49 ± 3
Volunteer 6	acc.	750 ± 51 / 48 ± 3	1391 ± 166 / 46 ± 3	801 ± 83 / 48 ± 5	749 ± 78 / 50 ± 4	722 ± 52 / 53 ± 6	833 ± 82 / 46 ± 3
	unacc.	787 ± 56 / 48 ± 3	1312 ± 208 / 44 ± 5	806 ± 77 / 47 ± 4	792 ± 46 / 51 ± 2	747 ± 46 / 49 ± 2	906 ± 71 / 47 ± 3

Table 1. T_1 and T_2 determination with SMS-TESS using acceleration factors of R=2 and R=4 is compared to single-slice TESS scans in four subjects for similar anatomical regions (R=2: ROI 1 in frontal WM / ROI 2 in GM (putamen), R=4: all ROIs in WM structures; for the definition of the ROI locations cf. Supporting Information Figure S2; generally, ROI n is defined on slice n; T_1 / T_2 in ms).
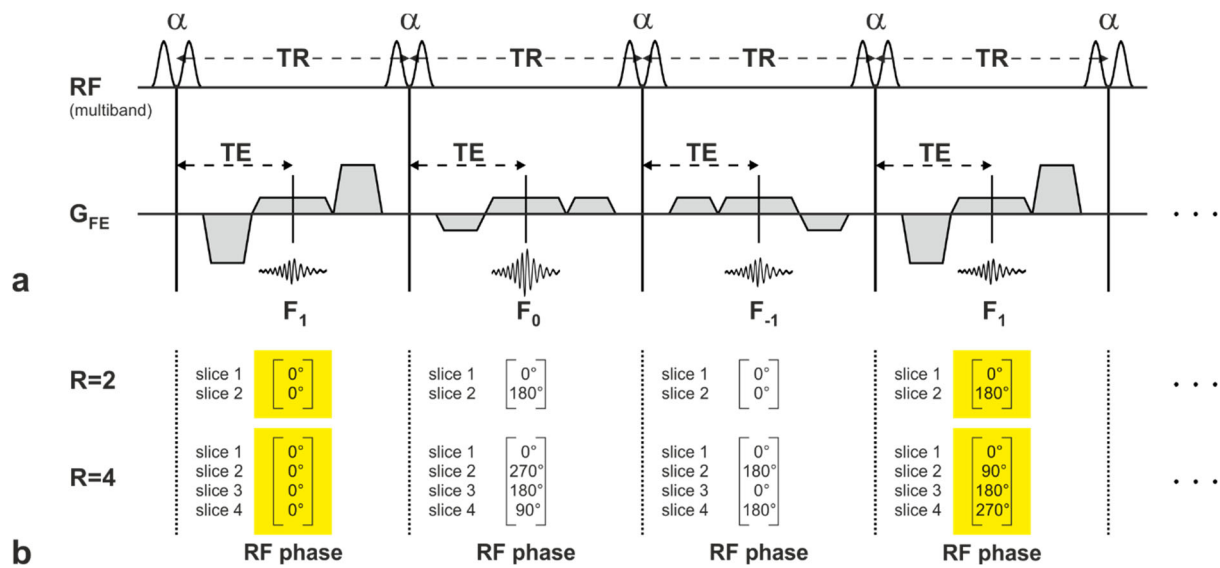
FIGURES

Figure 1. (**a**) SMS-TESS sequence scheme. Multiband RF pulses are employed to excite multiple slices simultaneously. The three SSFP contrasts (F_1, F_0, F_{-1}) are acquired in different RF cycles to ensure a short TR and thus to reduce the sensitivity to susceptibility. (**b**) According to the concept of 2D multislice CAIPIRINHA (15), alternating multiband RF pulses with different phase modulations are implemented. For an SMS acceleration factor of R=2, the depicted scheme of two alternating pulses ensures to label the two simultaneously excited slices with individual phase-cycles (slice 1: 0°, slice 2: 180°, as highlighted in yellow for the F_1 contrast). As a result, slice 2 is shifted by FOV/2 with respect to slice 1 in the aliased image. For R=4, the alternation of four RF pulses with proper phase modulations enables to provide slices 1, 2, 3, and 4 with phase-cycles of 0°, 90°, 180°, and 270°, respectively (highlighted in yellow for the F_1 contrast). According to their phase-cycles, slices 2, 3, and 4 are shifted by FOV/4, FOV/2, and 3FOV/4 with respect to slice 1. Note that the RF phase increment of consecutive pulses must be constant for each slice in order to maintain the F_1, F_0, and F_{-1} steady-state configurations needed for quantitative TESS imaging.
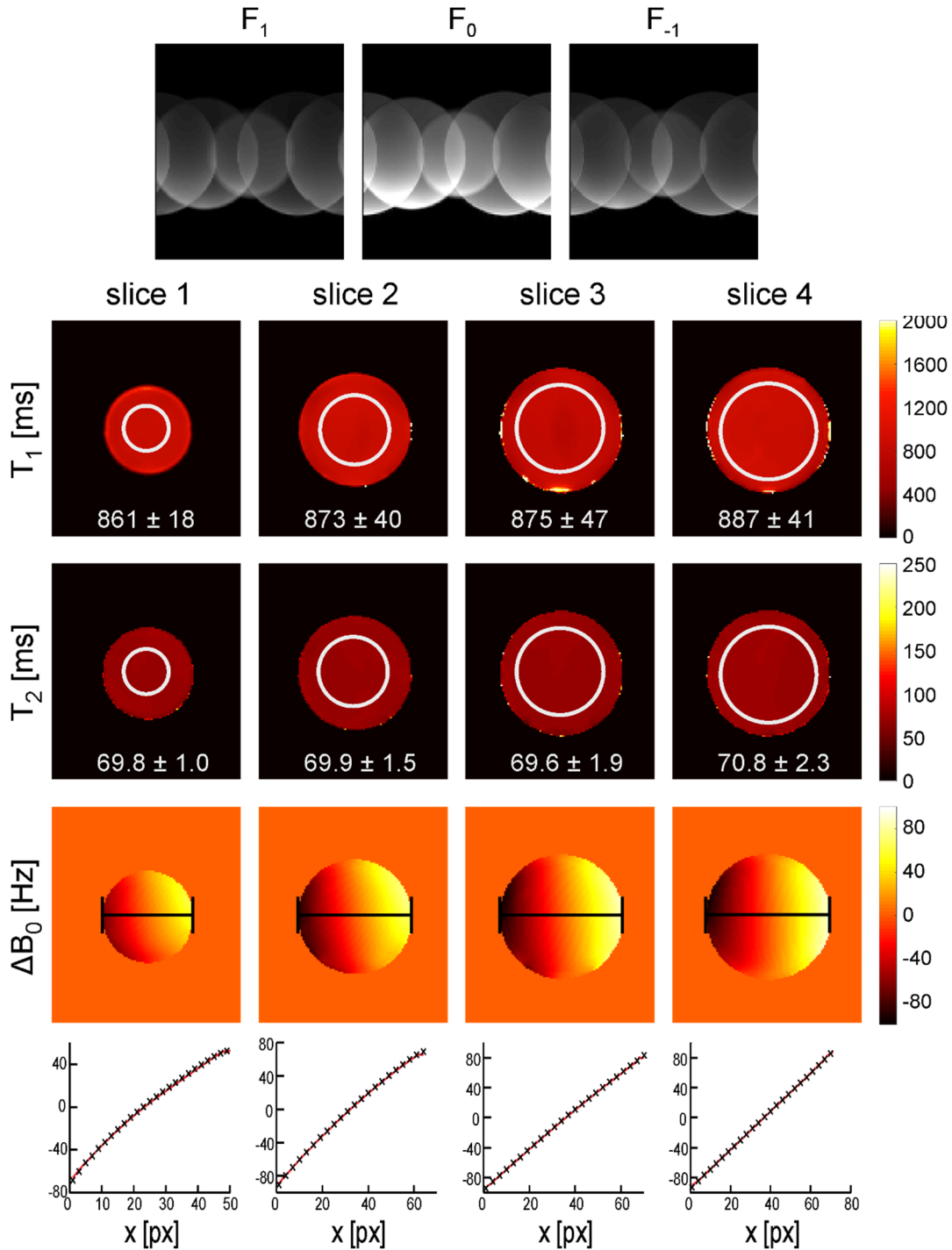
Figure 2. *In vitro* validation of SMS-TESS T_1, T_2, and ΔB_0 mapping for an acceleration factor of 4. Aliased TESS base contrasts are shown in the first row. The T_1 and T_2 maps calculated for the four slices acquired with SMS-TESS are displayed in the 2nd and 3rd row along with the assessed mean values for a circular ROI (white circles drawn directly on the maps). The corresponding off-resonance (ΔB_0) maps are shown in the 4th row. In the 5th row, SMS-TESS ΔB_0 values (black crosses) are plotted against the reference measurement (solid red curve) for the solid black line indicated on the off-resonance maps in the 4th row.
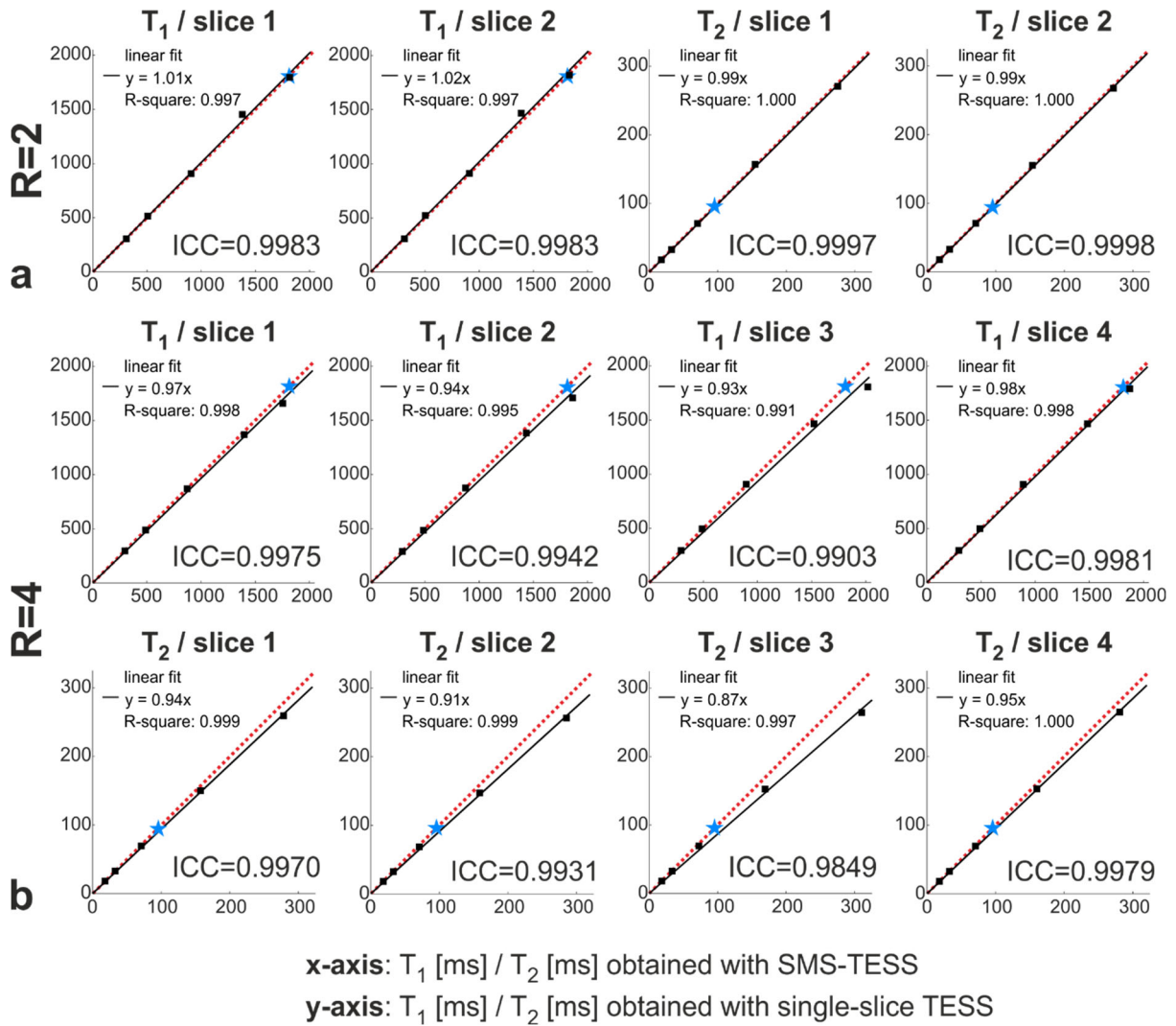
Figure 3. Validation of SMS-TESS relaxometry (x-axis) versus single-slice TESS relaxometry (y-axis) in five manganese-doped probes with different $MnCl_2$ concentrations (black squares) for acceleration factors of 2 (**a**) and 4 (**b**); individually performed for each acquired slice. The agreement between the two methods is evaluated by the calculation of the intraclass correlation coefficient (ICC) and linear least-squares fitting while forcing the y-intercept to 0 (solid black line). The dotted red line represents the reference line of perfect agreement (y = x). The blue star indicates the upper limit of T_1 and T_2 values reported for white and gray matter structures in the human brain at 3 T (28).
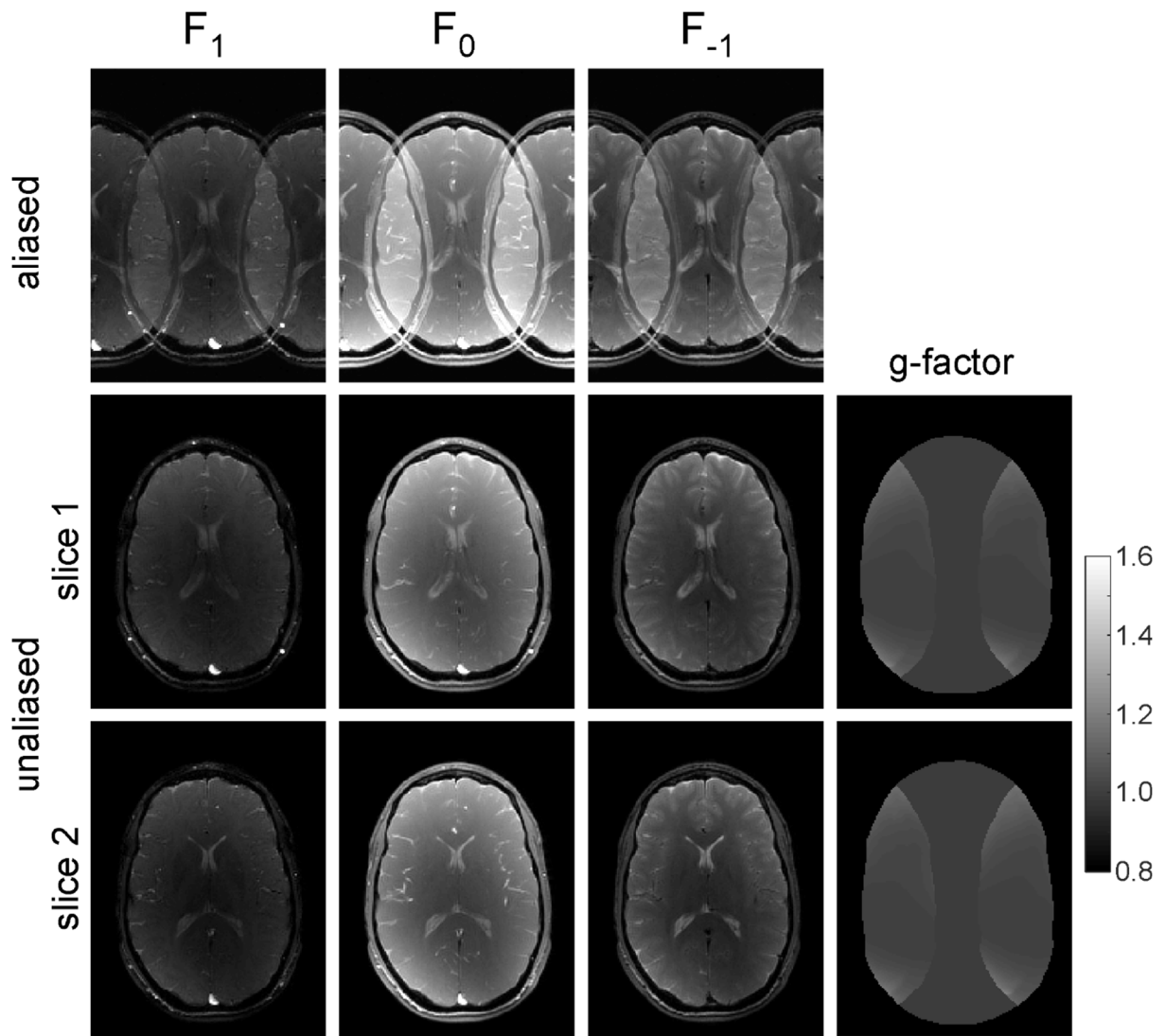
Figure 4. SMS-TESS imaging using CAIPIRINHA with an acceleration factor of 2 in the human brain at 3 T (volunteer 1). The aliased acquired TESS contrasts (F_1, F_0, and F_{-1}) are shown in the first row and the unfolded two slices with the corresponding g-factor maps in the 2nd (slice 1) and 3rd (slice 2) row.
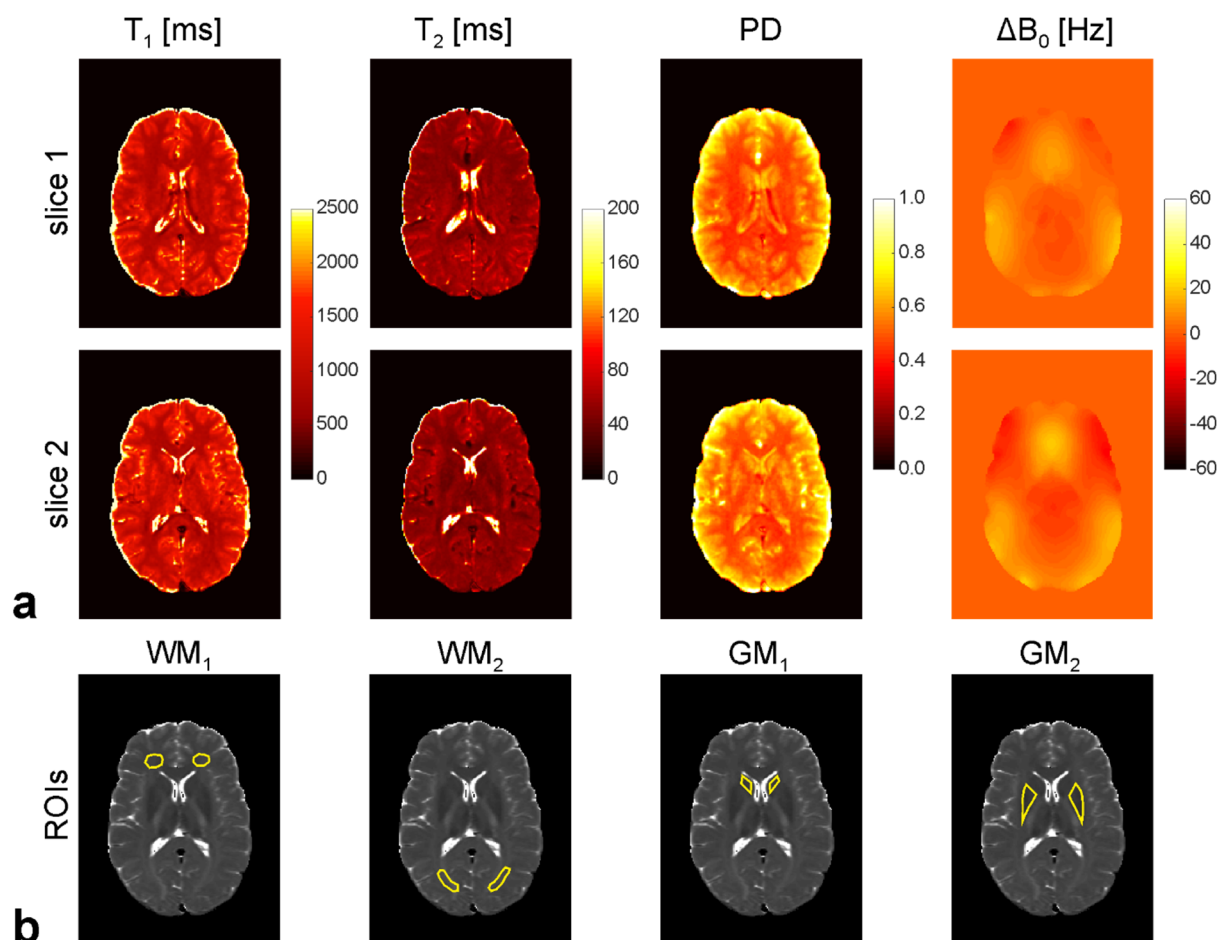
Figure 5. (**a**) Multiparametric SMS-TESS brain tissue characterization corresponding to the data set presented in Figure 4 (acceleration factor: R=2). Based on a single SMS-TESS measurement, quantitative maps of T_1, T_2, PD, and off-resonance frequency (ΔB_0) are obtained simultaneously for two slices in the human brain at 3 T (rows 1 and 2). (**b**) SMS-TESS T_1 and T_2 accuracy in the human brain is assessed for ROIs as indicated here on the reference T_2 map in frontal white matter (WM_1), occipital white matter (WM_2), the caudate nucleus head (GM_1), and the putamen (GM_2).
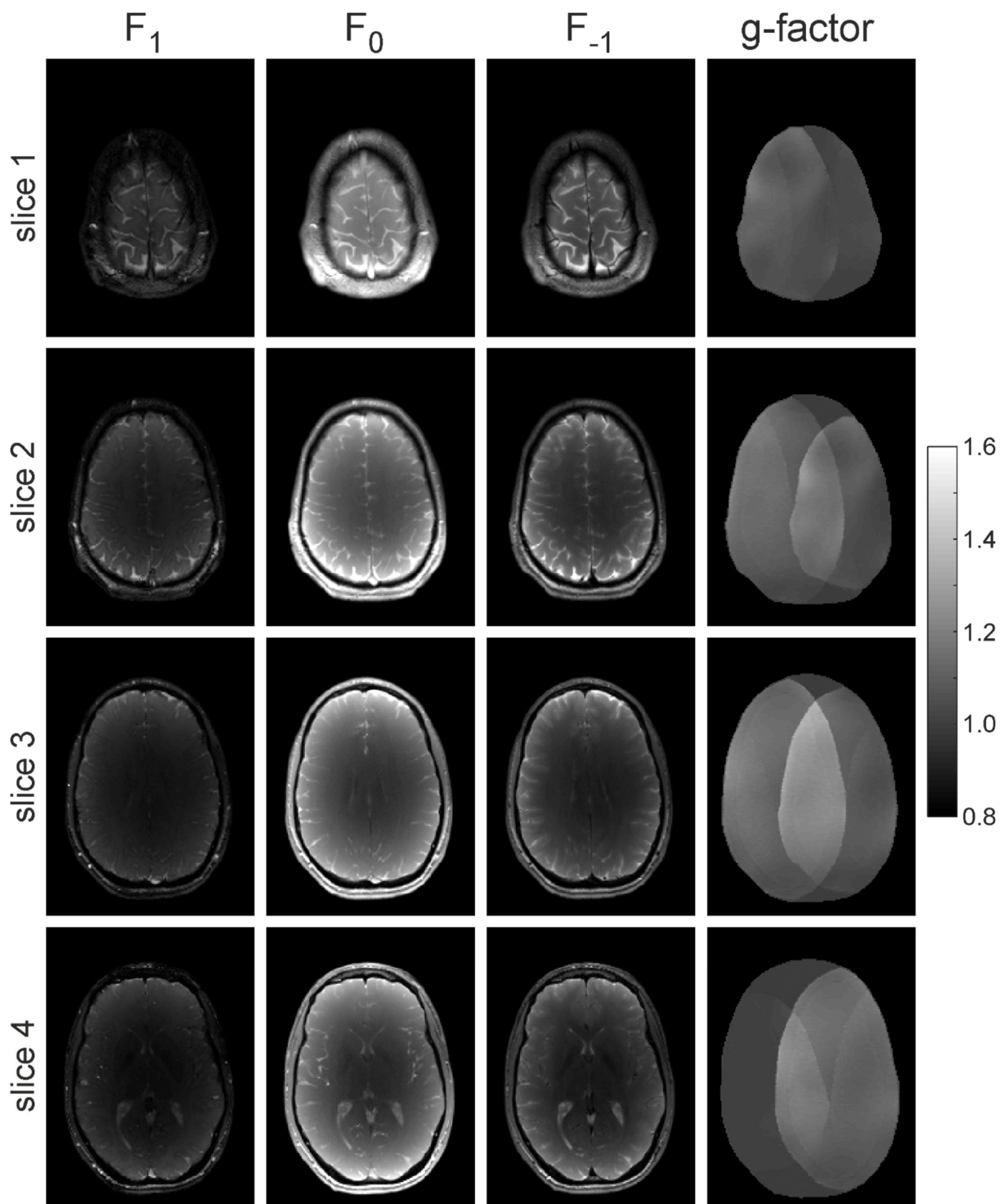
Figure 6. SENSE reconstruction results of SMS-TESS imaging with an acceleration factor of 4 shown here for a representative data set acquired in volunteer 1 at 3 T. The reconstructed (unfolded) four slices of the three TESS base images (F_1, F_0, F_{-1}) are provided along with their respective g-factor maps. The corresponding aliased base TESS contrasts are shown in the Supporting Information Figure S3.
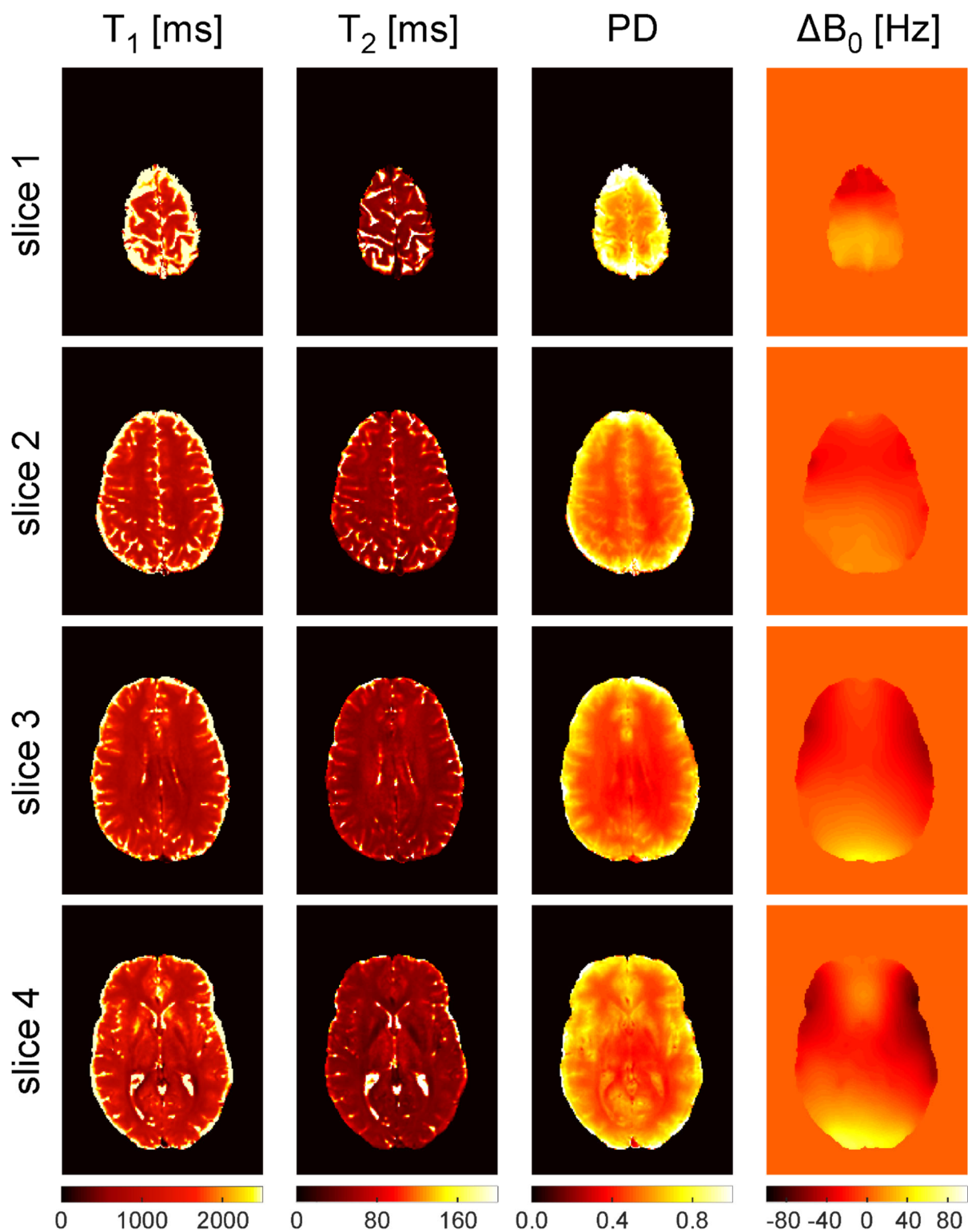
Figure 7. SMS-TESS brain tissue quantification with an acceleration factor of 4. The quantitative maps (T_1, T_2, PD, and ΔB_0) correspond to the data set displayed in Figure 6. Please note that for the T_1, T_2, and PD maps the same scaling was used as in Figure 5 while the scaling of the ΔB_0 map was slightly adapted in comparison to Figure 5 due to the increased range of mapped frequencies (resulting from a different shim setting).
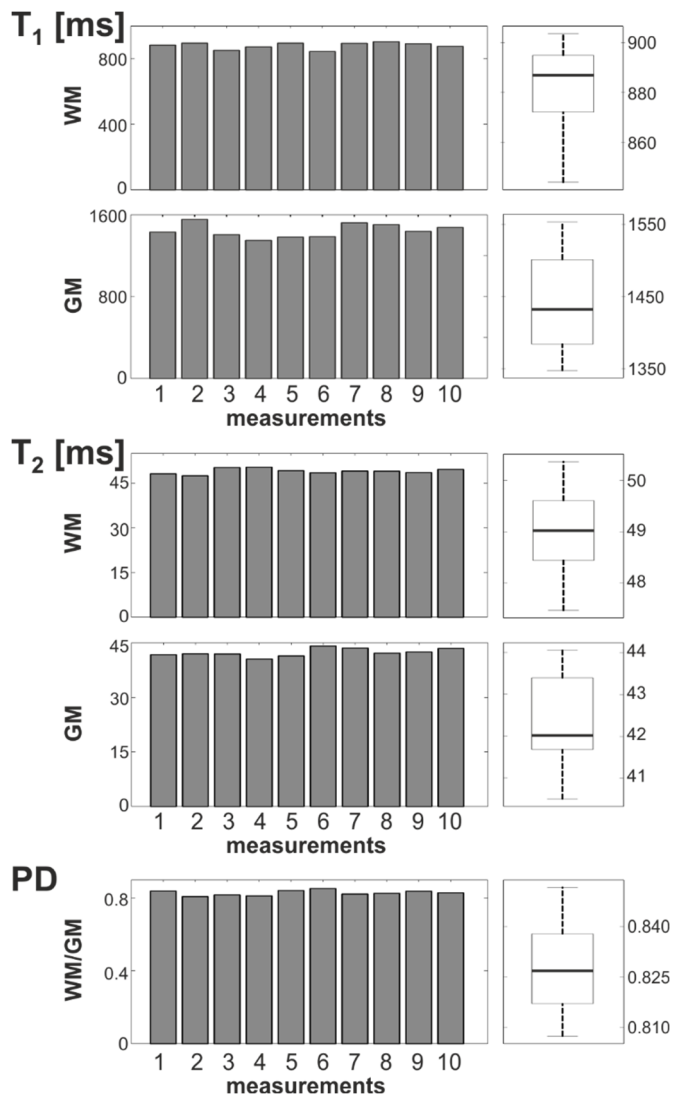
Figure 8. Reproducibility assessment in volunteer 2 for R=4 in a WM and a GM ROI defined on slice 4 (cf. Supporting Information Figure S1). The bar plots illustrate the T_1 and T_2 variability assessed in the WM and GM ROIs as well as the PD variability assessed as the ratio of the WM ROI to the GM ROI. The box plots on the right show the median values (thick solid line), lower and upper quartile values (bottom and top of the box) and the extent of the data from minimal to maximal values (dashed lines).
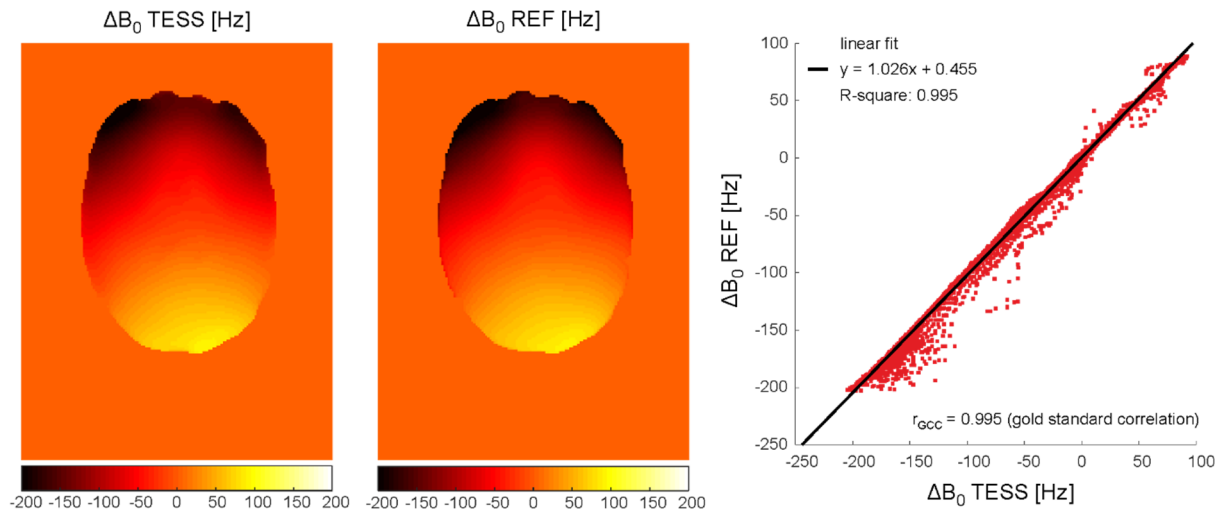
Figure 9. Left: representative ΔB_0 map obtained from SMS-TESS imaging with R=4 in volunteer 2 (slice 4, cf. Supporting Information Figure S1). Middle: reference ΔB_0 map obtained from a dual-echo gradient echo scan. Right: correlation scatter plot with a linear fit (solid black line) yielding a slope close to 1 (a value of 1 would indicate perfect agreement). The excellent agreement between the two methods is reflected by a high gold standard correlation coefficient of 0.995.
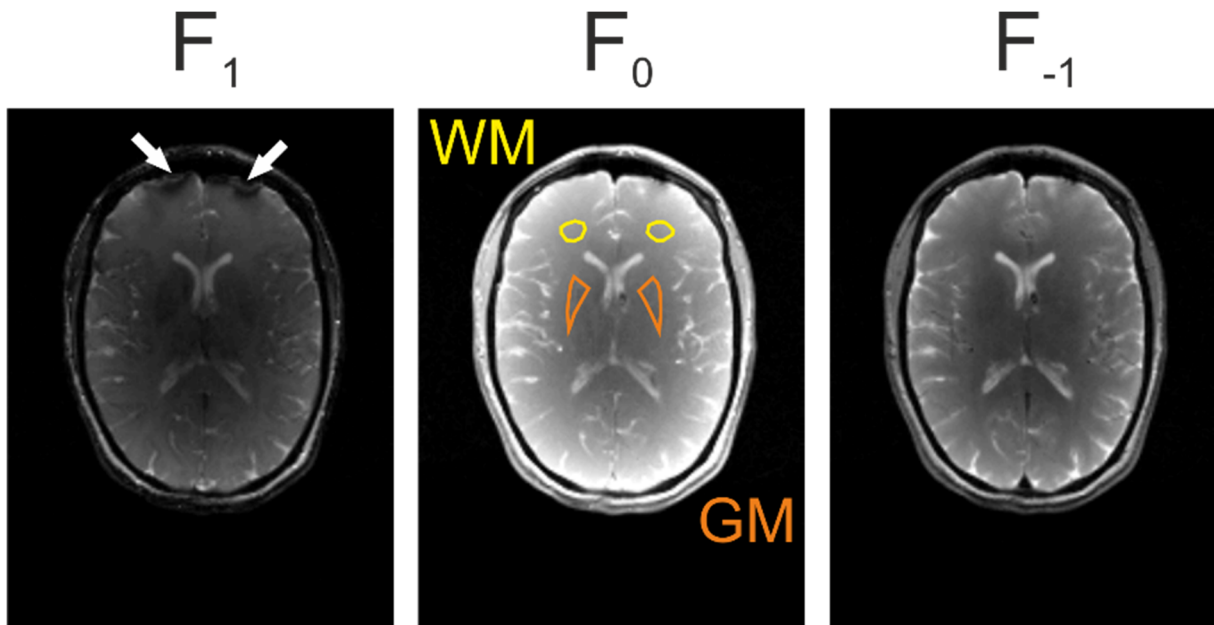
SUPPORTING INFORMATION

*Validation in a phantom with four different T_1 and T_2 compartments*

A phantom was prepared that consisted of four small tubes containing different concentrations of $MnCl_2$ diluted in water. The tubes were separated by a center-to-center distance of 2 cm and emerged in a water bath. SMS-TESS images were acquired with a center-to-center slice gap of 2 cm for both R = 2 and R = 4 such that in each slice a different compartment could be assessed. At R = 2, two measurements were performed with different slice positioning to assess all four compartments. The matrix size was set to 128 x 120 yielding a total scan time of 21 s (otherwise all parameters were identical to the *in vitro* protocol described in the "Methods" section). The reference T_1 was derived from eight single-slice inversion-recovery turbo-spin-echo scans with a TR of 10 s and inversion times of TI = [50, 100, 200, 400, 800, 1600, 3200, 6400] ms by nonlinear least-squares fitting of the acquired data sets. The reference T_2 was derived from eight single-slice single-echo spin-echo scans with a TR of 5000 ms and echo times of TE = [7.5, 12, 20, 40, 70, 100, 200, 400] ms using nonlinear least-squares fitting. The results are summarized in the **Supporting Information Table S1**.

|	T_1 / T_2 in [ms]		
	SMS-TESS R=2	*SMS-TESS R=4*	*Reference*
Compartment 1	775 ± 45 / 58 ± 2	847 ± 138 / 60 ± 4	765 ± 20 / 57 ± 2
Compartment 2	974 ± 67 / 75 ± 2	1013 ± 150 / 83 ± 11	936 ± 30 / 74 ± 2
Compartment 3	1228 ± 139 / 107 ± 5	1298 ± 192 / 112 ± 12	1210 ± 52 / 108 ± 5
Compartment 4	1377 ± 143 / 139 ± 8	1449 ± 152 / 141 ± 11	1397 ± 67 / 143 ± 3

Supporting Information Table S1. Comparison of SMS-TESS relaxometry with R = 2 and R = 4 against standard reference data.

Supporting Information Figure S1. Representative unaliased base TESS images of slice 4 acquired in volunteer 2 at 3T in the course of 10 consecutive SMS-TESS measurements with $R = 4$. Note the susceptibility sensitivity of the F_1 contrast that results in some artifacts near the sinuses (white arrows, left). The WM and GM ROIs used for reproducibility assessment are indicated on the F_0 contrast (middle).
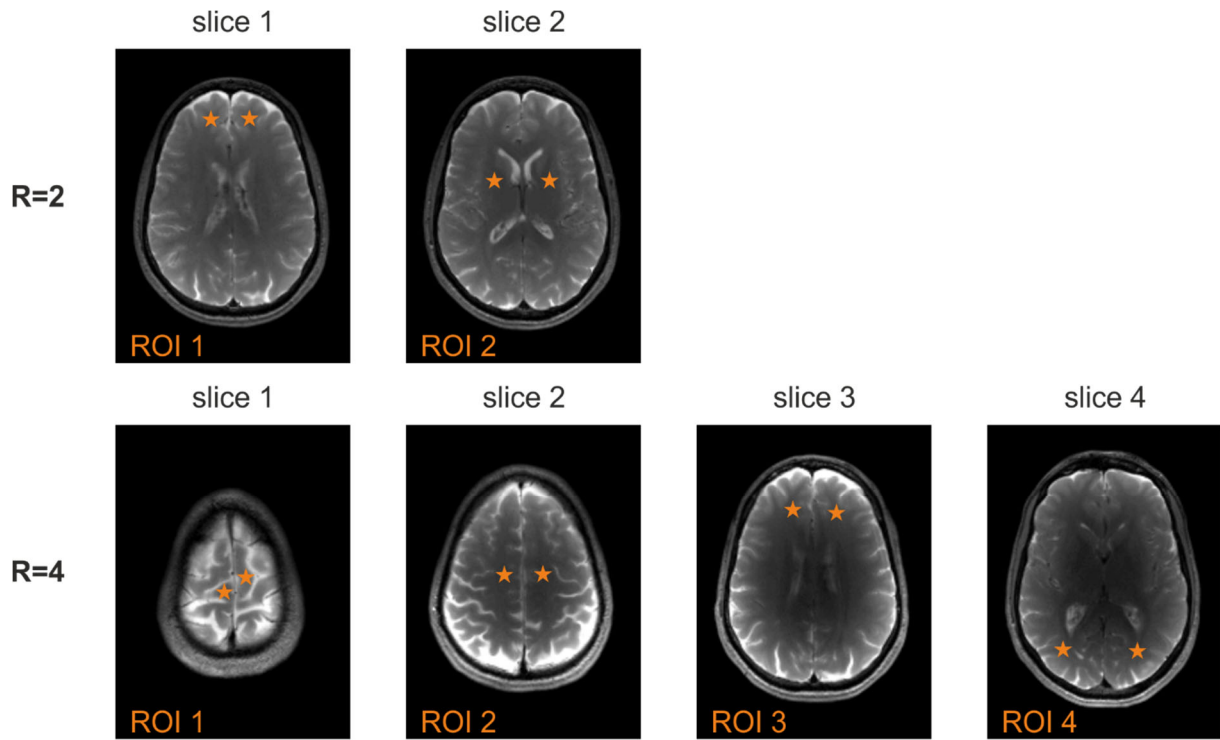
Supporting Information Figure S2. The location of the ROIs used for the T_1 and T_2 comparison between SMS-TESS and single-slice TESS is indicated on the unfolded F_{-1} base images acquired in volunteer 6 with acceleration factors of 2 (first row) and 4 (second row).
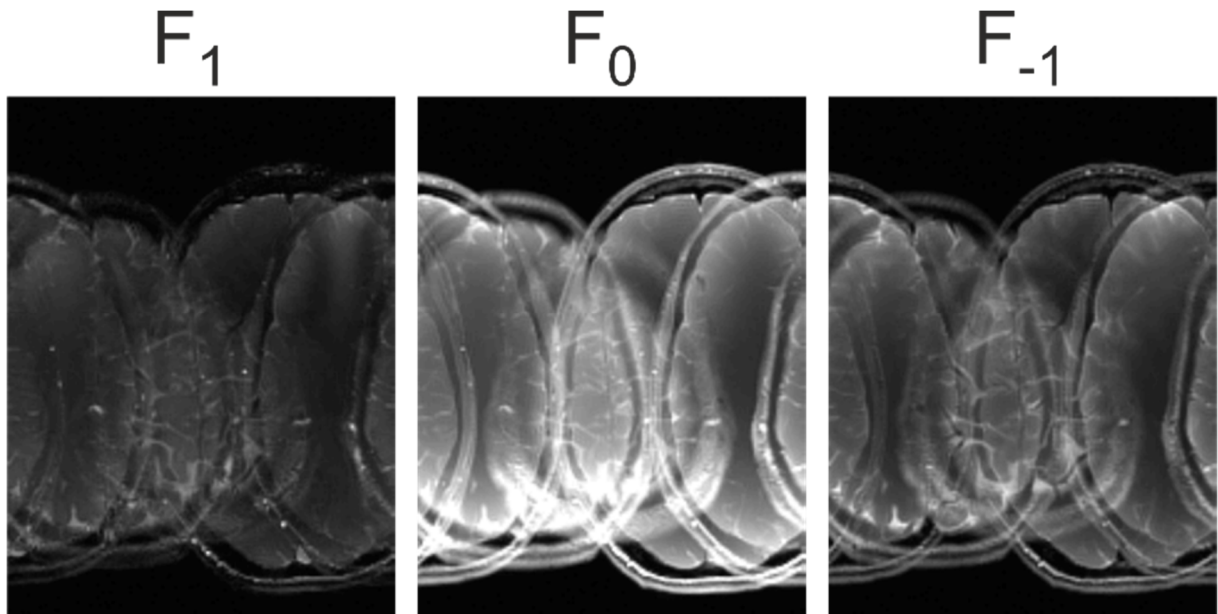
Supporting Information Figure S3. Simultaneous excitation of four slices with SMS-TESS following the concept of CAIPIRINHA results in highly aliased TESS base images (F_1, F_0, F_{-1}) as shown here for a data set acquired in volunteer 1 at 3T. The aliased data set corresponds to the unfolded TESS base images presented in Figure 6.